Technical Note

Occurrence and Characteristic Frequencies of Nappe Oscillations at Free-Overfall Structures

Vasileios Kitsikoudis[1]; Maurine Lodomez[2]; Benjamin Dewals[3]; Pierre Archambeau[4]; Michel Pirotton[5]; and Sebastien Erpicum, A.M.ASCE[6]

Abstract: The present study investigated the occurrence and characteristic frequency of nappe oscillations on weirs by reanalyzing data from 52 experimental configurations. The considered configurations include various shapes of the weir crest and a range of weir geometric and hydraulic characteristics with two different scales. Nappes were either confined with lateral and back walls forming a nonvented air pocket between the nappe and the weir or unconfined with atmospheric pressure everywhere around the nappe. Oscillations occurred at nappes with uniformly distributed approaching flow of low velocity and unit discharge between 0.01 and 0.06 m^2/s, regardless of the model scale. Weir crests that favored nappe oscillations had an upstream profile without geometric discontinuities. A dimensionless frequency of nappe oscillations was expressed as a power function of the ratio of the fall height to the water depth at the point of detachment at the crest, separately for quarter-round and truncated half-round weir crests. The exponents of the two obtained power functions were very close to each other, which allows the usage of their average so that different weir crests exhibit solely offsetting curves. **DOI: 10.1061/(ASCE)HY.1943-7900.0001839.**

Author keywords: Experimental hydraulics; Hydraulic model; Nappe oscillations; Weir.

Introduction

The water overflowing a weir crest forms a thin sheet known as nappe that heads downwards in free fall. The nappe may become unstable and exhibit vibrations or oscillations when the approaching hydraulic head is relatively low and the flow distribution is uniform (Lodomez et al. 2018). Nappe oscillations are characterized by horizontal bands covering the whole width of the nappe with an undulated pattern. Nappe oscillations are particularly undesirable because they may cause vibrations in the hydraulic structure (Petrikat 1958) and create a tremendous amount of noise with severe environmental consequences and adverse impacts on people living nearby (Crookston et al. 2014). The cause of these oscillations is still not fully understood, and therefore, there is a need to investigate the flow processes leading to nappe oscillations.

Anderson and Tullis (2018) observed that nappe oscillations depend on the unit discharge and not on the weir scale, which suggests that the phenomenon cannot be modeled with Froude similarity. Anderson and Tullis (2018) noted that nappe oscillations on a small-scale weir occurred more erratically and intermittently than on a large-scale weir. Khodier and Tullis (2018) conducted particle image velocimetry measurements during intermittent periods of nappe oscillations and showed that the flow velocity pattern near a quarter-round weir crest remained similar for oscillating and nonoscillating periods of the nappe. Chanson (1996) attributed the formation of nappe oscillations to the abrupt pressure change at the detachment point of the crest, where the pressure suddenly decreases. The role of the flow conditions on the weir crest was also highlighted by Anderson and Tullis (2018), who observed that an increase in crest roughness impedes the formation of nappe oscillations. Casperson (1993) suggested that nappe oscillations occur due to shear and the resulting Kelvin-Helmholtz instabilities at the interface between the flowing water in the nappe and the surrounding air, while Naudascher and Rockwell (1994) considered the pressure fluctuations in the air pocket behind the nappe as a driving mechanism. Oscillations have been observed both at confined and unconfined nappes, i.e., at nappes that were bounded at their sides and their back leading to nonvented air pockets and nappes that were fully exposed to atmospheric pressure, respectively. However, confined nappes exhibit more stable and enhanced oscillations compared to unconfined nappes (Anderson and Tullis 2018). Schmid and Henningson (2002) expressed nappe oscillations as a linear combination of global modes, while other theoretical approaches have considered nappe oscillations to behave like a mass-spring model, with the nappe and the enclosed air pocket

[1]Postdoctoral Researcher, Urban and Environmental Engineering, Hydraulics in Environmental and Civil Engineering, Liege Univ. Quartier Polytech, Allée de la Découverte 9, Bat B52/3 +1, B-4000 Liège, Belgium (corresponding author). Email: v.kitsikoudis@uliege.be; v.kitsikoudis@utwente.nl

[2]Engineer, SBE-Wallonie, Namur Office Park, Ave. des Dessus-de-Lives 2, 5101 Namur, Belgium. Email: maurine.lodomez@gmail.com

[3]Professor, Urban and Environmental Engineering, Hydraulics in Environmental and Civil Engineering, Liege Univ. Quartier Polytech, Allée de la Découverte 9, Bat B52/3 +1, B-4000 Liège, Belgium. Email: b.dewals@uliege.be

[4]Research Associate, Urban and Environmental Engineering, Hydraulics in Environmental and Civil Engineering, Liege Univ. Quartier Polytech, Allée de la Découverte 9, Bat B52/3 +1, B-4000 Liège, Belgium. ORCID: https://orcid.org/0000-0001-7712-3453. Email: pierre.archambeau@uliege.be

[5]Professor, Urban and Environmental Engineering, Hydraulics in Environmental and Civil Engineering, Liege Univ. Quartier Polytech, Allée de la Découverte 9, Bat B52/3 +1, B-4000 Liège, Belgium. ORCID: https://orcid.org/0000-0002-2483-5489. Email: michel.pirotton@uliege.be

[6]Associate Professor, Urban and Environmental Engineering, Hydraulics in Environmental and Civil Engineering, Liege Univ. Quartier Polytech, Allée de la Découverte 9, Bat B52/3 +1, B-4000 Liège, Belgium. ORCID: https://orcid.org/0000-0002-7094-9604. Email: s.erpicum@uliege.be

Note. This manuscript was submitted on February 19, 2020; approved on August 14, 2020; published online on November 28, 2020. Discussion period open until April 28, 2021; separate discussions must be submitted for individual papers. This technical note is part of the ***Journal of Hydraulic Engineering***, © ASCE, ISSN 0733-9429.

behind a confined nappe corresponding to the inertia effects and the spring, respectively (De Rosa et al. 2014; Girfoglio et al. 2017).

Nappe oscillations are broadly characterized by their frequency, which is affected considerably by the geometric characteristics of the weir, such as the crest type and the fall height (Lodomez et al. 2019b). However, so far, there have been no established relationships linking the characteristic frequencies of nappe oscillations to geometric and hydraulic parameters of the weir. To this end, the aim of this study is to analyze experimental data to (1) determine the conditions (crest type, weir geometry, and hydraulics) under which nappe oscillations occur, and (2) provide for the first time a predictive formula linking the dominant frequency of nappe oscillations to the weir characteristics. The analysis is based on laboratory experimental results from 52 configurations. All of the data have been recently published in open access by Lodomez et al. (2020). Data from five configurations have already been partly analyzed by Lodomez et al. (2018, 2019b), while the data from the 47 remaining configurations are analyzed for the first time in this paper in which the dataset is exploited for the derivation of a quantification formula for the nappe oscillations frequency.

Methods and Experimental Data

A series of experiments was conducted in a large-scale linear weir at the Engineering Hydraulics Laboratory at the University of Liege in Belgium (Model 1) and in a small scale model at the Utah Water Research Laboratory at Utah State University in the US (Model 2). In total, 52 different configurations (44 in Model 1 and 8 in Model 2) are analyzed in this study, with varying hydraulic parameters, weir geometric characteristics, and crest profiles, as well as with or without nappe confinement (Table 1).

Five geometries were tested for the weir crest profile: quarter-round (QR), half-round (HR), truncated half-round (THR), rectangular (R), and rounded rectangular (RR) crests (Fig. 1). Experiments in the large-scale model were carried out with QR, THR, and HR crests with a radius of 15 cm. For the small-scale model experiments, the QR and THR crests that were tested had a 5 cm radius. R and RR crests were tested only in the small-scale model. As shown in Table 1, the tested fall heights L and crest widths W in the large-scale Model 1 were varied in the ranges of 0.5–3 m and 1–3.45 m, respectively. In the small-scale Model 2, the fall height was varied between 0.5 and 1 m, while the crest width was kept constant at 1.2 m. A wide range of incoming unit discharges was tested for each configuration. The experiments with QR and THR crests from Model 2 with a fall height equal to 1 m and from Model 1 with a width of 3.45 m have been discussed in other studies (Lodomez et al. 2018, 2019b), although from a different perspective than the present study. The rest of the configurations in Table 1 are analyzed in this study for the first time.

The flow discharges were measured with electromagnetic flowmeters and the associated water levels with point gauges. The characteristic frequencies of nappe oscillations were determined from acoustic measurements and image processing. The acoustic measurements in Model 1 were conducted with a free-field microphone MC212 (Metravid, Limonest, France) and in Model 2 with a free-field microphone Behringer ECM8000 (Behringer GmbH, Willich, Germany). The dominant frequency was determined with spectral analysis with a Hanning window with 50% overlap. Two high-speed cameras were used for image acquisition for both models, a GoPro Hero 4 (240 Hz) (GoPro, San Mateo, California) and an Imager MX4M Lavision (300 Hz) (Lavision, Goettingen, Germany). The image analysis aimed to detect the motion of visible horizontal bands that were discernible from the lighting on the nappe undulations. Monitored pixels varied between white for lit bands and black for unlit bands in the grayscale, and the fast Fourier transform of the obtained time-series generated the associated frequency of the nappe oscillations. All instruments were positioned in front of the nappe, facing the centerline of the weir. The obtained frequencies from the video and sound measurements were identical (Lodomez et al. 2018). Measurements started either at a very low unit discharge, which was progressively and slowly increasing until nappe oscillations occurred or, alternatively, at a fairly high unit discharge with no nappe oscillations, which was gradually decreasing until nappe oscillations were observed. Subsequently, the unit discharge kept increasing or decreasing, depending on the initial unit discharge, and the frequency of nappe oscillations was measured at each step. This process was iterated until the unit discharge was too large or too small for nappe oscillations to occur. More details about the experiments are given by Lodomez et al. (2018, 2020), and the whole dataset is available open access in the study by Lodomez et al. (2020).

Dimensionless variables are needed for sound comparison of the results obtained from different geometries and from experimental setups at different scales. A dimensional analysis was carried out with the following ten variables: fall height, L; weir width, W; water depth at the crest point where the flow is detached, e; characteristic frequency of nappe oscillations, f; unit discharge of the flow approaching the crest, q; gravitational acceleration, g; fluid density, ρ; surface tension, σ; dynamic viscosity of the fluid, μ; and characteristic velocity of the nappe, v, which is defined as the difference between the free-fall vertical velocity of the nappe at the impact and at the point of detachment at the crest, ($v = \sqrt{v_0^2 + 2gL} - v_0$, with v_0 as the vertical flow velocity at the nappe detachment point). This expression of the characteristic velocity has been proposed by Schwartz (1964).

The dimensional analysis generated the following seven dimensionless variables: L/e, W/e, fe/v, $q/(ve)$, $v/(ge)^{0.5}$, $\rho v^2 e/\sigma$, and $\rho ve/\mu$. The last three variables are the Froude, Weber, and Reynolds numbers, respectively. The configurations and tests analyzed in this paper cover a large range of these seven dimensionless variables, with the maximum value being at least five times greater than the minimum value.

Results and Discussion

Nappe oscillations were observed in 34 out of 52 tested configurations (Table 1) for uniformly distributed approaching flows with unit discharge q ranging from 0.01 to 0.06 m^2/s for the vast majority of cases. The corresponding upstream head varied from 0.03 to 0.12 m, with the oscillations gradually vanishing as the upstream head increased above or decreased below a certain value. A hysteresis effect on nappe oscillations occurrence was observed only on Model 2 for discharges lower than 0.02 m^2/s (Lodomez et al. 2019b), despite the fact that the nappe was always detached from the weir wall.

The weir crest profile has a substantial influence on whether or not the nappe oscillations occur. For the large-scale Model 1, when geometry was kept constant with 3-m fall height and 3.45-m width, nappe oscillations occurred for QR and THR crest profiles but not for the HR crest profile. A notable difference between the HR crest and the QR and THR crests lies in the fact that in QR and THR crests, the nappe detachment occurs at a sharp edge of the weir crest, which is not necessarily the case for the HR crest (Fig. 1). Nappe detachment in the HR crest occurs less abruptly, as the pressure gets further reduced toward atmospheric pressure (or entrapped air pocket pressure in case of confinement) along the crest

Table 1. Summary table of experimental setups, geometries, and the number of observations with oscillations development, n

No.	Model	Crest	W (m)	L (m)	n	q (m^2/s)	f (Hz)	Data analyzed in previous studies
1	1	QR (C)	3.45	3.00	203	0.029 ± 0.012	33.0 ± 1.8	Lodomez et al. (2018, 2019b)
2	1	THR (C)	3.45	3.00	132	0.037 ± 0.014	19.9 ± 11.2	Lodomez et al. (2019b)
3	1	THR (C)	3.45	2.50	77	0.027 ± 0.011	19.3 ± 10.1	—
4	1	THR (C)	3.45	2.00	65	0.021 ± 0.008	19.3 ± 7.0	—
5	1	THR (C)	3.45	1.50	36	0.017 ± 0.006	20.7 ± 6.5	—
6	1	THR (C)	3.45	1.00	49	0.038 ± 0.013	19.6 ± 1.0	—
7	1	THR (C)	2.50	3.00	57	0.024 ± 0.007	19.8 ± 4.8	—
8	1	THR (C)	2.50	2.50	60	0.020 ± 0.008	22.1 ± 4.7	—
9	1	THR (C)	2.50	2.00	59	0.015 ± 0.004	17.0 ± 6.1	—
10	1	THR (C)	2.50	1.50	0	—	—	—
11	1	THR (C)	2.00	3.00	50	0.023 ± 0.008	14.6 ± 5.9	—
12	1	THR (C)	2.00	2.50	42	0.022 ± 0.008	12.9 ± 5.7	—
13	1	THR (C)	2.00	2.00	20	0.014 ± 0.004	16.2 ± 0.6	—
14	1	THR (C)	2.00	1.50	0	—	—	—
15	1	THR (C)	1.50	3.00	34	0.021 ± 0.005	20.4 ± 3.0	—
16	1	THR (C)	1.50	2.50	42	0.021 ± 0.008	14.4 ± 0.6	—
17	1	THR (C)	1.50	2.00	35	0.014 ± 0.003	24.4 ± 13.4	—
18	1	THR (C)	1.50	1.50	0	—	—	—
19	1	THR (C)	1.00	3.00	15	0.016 ± 0.002	22.7 ± 0.4	—
20	1	THR (C)	1.00	2.50	61	0.022 ± 0.008	21.7 ± 0.7	—
21	1	THR (C)	1.00	2.00	12	0.013 ± 0.003	21.8 ± 13.0	—
22	1	THR (C)	1.00	1.50	0	—	—	—
23	1	HR (C)	3.45	3.00	0	—	—	—
24	1	HR (C)	3.45	1.00	55	0.022 ± 0.010	39.8 ± 8.9	—
25	1	HR (C)	3.45	0.50	76	0.025 ± 0.010	37.5 ± 2.6	—
26	1	QR (UC)	3.45	3.00	310	0.031 ± 0.009	40.2 ± 6.0	Lodomez et al. (2018)
27	1	QR (UC)	3.45	2.50	44	0.026 ± 0.011	41.9 ± 5.5	—
28	1	QR (UC)	3.45	2.00	103	0.023 ± 0.010	35.4 ± 6.7	—
29	1	QR (UC)	3.45	1.50	0	—	—	—
30	1	QR (UC)	3.45	1.00	0	—	—	—
31	1	QR (UC)	3.45	0.50	0	—	—	—
32	1	QR (UC)	2.50	3.00	79	0.018 ± 0.009	49.8 ± 3.9	—
33	1	QR (UC)	2.50	2.50	75	0.024 ± 0.010	39.0 ± 7.4	—
34	1	QR (UC)	2.50	2.00	103	0.023 ± 0.009	33.9 ± 4.3	—
35	1	QR (UC)	2.50	1.50	0	—	—	—
36	1	QR (UC)	2.50	0.50	0	—	—	—
37	1	QR (UC)	2.00	2.00	2	0.023 ± 0.003	35.0 ± 0.3	—
38	1	QR (UC)	2.00	1.50	0	—	—	—
39	1	QR (UC)	2.00	1.00	0	—	—	—
40	1	QR (UC)	2.00	0.50	0	—	—	—
41	1	QR (UC)	1.50	3.00	54	0.016 ± 0.004	49.9 ± 2.6	—
42	1	QR (UC)	1.50	2.50	28	0.013 ± 0.002	29.8 ± 0.1	—
43	1	QR (UC)	1.50	2.00	0	—	—	—
44	1	QR (UC)	1.00	3.00	0	—	—	—
45	2	QR (C)	1.20	1.00	134	0.034 ± 0.012	39.6 ± 3.8	Lodomez et al. (2019b)
46	2	QR (C)	1.20	0.75	73	0.035 ± 0.011	38.8 ± 4.3	—
47	2	QR (C)	1.20	0.50	0	—	—	—
48	2	THR (C)	1.20	1.00	79	0.033 ± 0.011	47.8 ± 6.8	Lodomez et al. (2019b)
49	2	THR (C)	1.20	0.75	25	0.039 ± 0.006	48.5 ± 1.7	—
50	2	THR (C)	1.20	0.50	0	—	—	—
51	2	R (C)	1.20	1.00	0	—	—	—
52	2	RR (C)	1.20	1.00	18	0.023 ± 0.002	40.0 ± 1.7	—

Note: In the crest column, confined and unconfined nappes are denoted by C and UC in the parenthesis, respectively. The unit discharge of the approaching to the crest flow and the frequency of nappe oscillations are given as mean value ± one standard deviation.

until the point where the nappe detaches. For all other weir crests, the detachment point is imposed by the crest geometry at the sharp downstream edge (Fig. 1) and is less controlled by the approaching flow characteristics. At such abrupt geometric discontinuities, sudden pressure differences are anticipated that could lead to nappe oscillations (Chanson 1996).

In the case of the small-scale Model 2, nappe oscillations were observed with a 1-m fall height and 1.2-m width for the QR, THR, and RR crest profiles but not for the R crest profile. The fact that no nappe oscillations were observed for the R weir crest may be attributed to its edgy upstream geometry, which is radically different from the other crests (Fig. 1). Such a crest disrupts the flow over the crest and hinders the formation of consistent oscillations across the width of the nappe. A similar finding was reported by Anderson and Tullis (2018), who impeded the formation of nappe oscillations by increasing the roughness of a quarter-round crest, and Lodomez et al. (2019a), who prevented oscillations development by adding bolts on the upstream face of the crest. In all these cases, the flow turbulence on the crest increased, and this could be the reason that nappe oscillations did not occur.

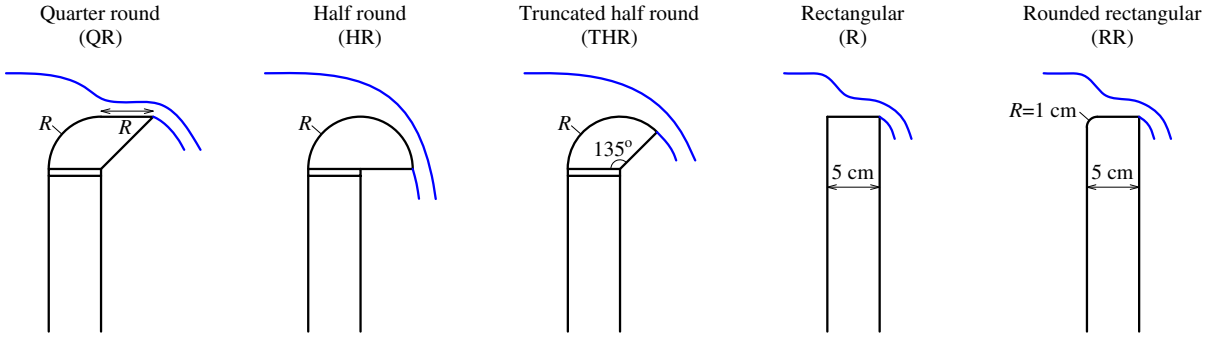

Fig. 1. Five different crest geometries tested in the experiments. The radius R in QR, HR, and THR crests is equal to 15 cm for Model 1 and 5 cm for Model 2.

The effect of L and W on the formation of nappe oscillations appears more erratic, as can be inferred from Table 1. For Model 1, nappe oscillations occur for relatively large values of these variables. For example, for the QR crest and unconfined nappe, nappe oscillations were observed for $L \geq 2$ m and $W \geq 1.5$ m. For the THR crest with confined nappe, oscillations were observed for all tested crest widths provided that $L \geq 2$ m, while for $L < 2$ m, nappe oscillations were observed only for the largest tested weir width (i.e., $W = 3.45$ m). For a fixed weir crest, nappe oscillations were observed in Model 2 for smaller fall heights than in Model 1.

The frequencies f of nappe oscillations depend primarily on the upstream unit discharge q, the confinement or not of the nappe, and the weir crest profile (Lodomez et al. 2018). The obtained frequencies of nappe oscillations are shown in Table 1. For Model 1 with a QR crest and unconfined nappe, the influence of the fall height on the frequency of nappe oscillations becomes stronger when the width of the weir is decreased. Indeed, for a width equal to 3.45 m, the frequencies remain relatively unchanged as the fall height decreases from 3 to 2 m. In contrast, a decreasing trend in the frequencies with a decrease in fall heights can be distinguished for widths equal to 2.50 and 1.50 m. The variations of the frequency of nappe oscillations for weirs with a THR crest and confined nappe are rather erratic, and no noticeable patterns could be detected.

Possible correlations between the seven dimensionless variables defined in the "Methods and Experimental Data" section and their combinations were systematically explored. The most satisfactory correlation was observed between the ratio L/e and a dimensionless frequency of nappe oscillations defined as $F = fq/v^2$, which is the product of the third and fourth of the aforementioned dimensionless variables. The relationship between the two dimensionless variables for weirs with the QR crest is shown in Fig. 2, with the data exhibiting a distinct power-law pattern that fits the data remarkably well, with the coefficient of determination $R^2 = 0.96$. Notably, the fitted curve covers a wide range of hydraulic and geometric characteristics from the two models at different scales, and oscillation frequencies vary by up to an order of magnitude. This trend is observed despite the fact that the crest width is not included in the considered dimensionless variables.

For some geometric configurations of the weir with a THR crest, data analysis revealed the existence of more than one dominant frequency for similar unit discharges. This wide range of dominant frequencies is attributed to harmonics of the signal and the fact that the signal processing algorithm captured a series of frequencies that are multiples of the lowest or fundamental frequency. This pattern was observed in nine out of the 19 experimental configurations with a THR crest where nappe oscillations occurred. To avoid subjectivity, data fitting was carried out by using only the data of the 10 configurations that did not present harmonics. The least-squares fit derived a power-law equation again with a very good fit to the data ($R^2 = 0.95$) [Fig. 3(a)]. Subsequently, all data with the THR crest were plotted in Fig. 3(b), from which it can be inferred that the harmonics led to a scatter of the data for specific L/e values. To further investigate this, Fig. 4 presents an example of one weir geometry with a THR crest that did not exhibit harmonics and one that did. For $W = 1.00$ m and $L = 2.50$ m, there were no harmonics present [Fig. 4(c)], and the data collapsed on a single curve when plotted in the dimensionless form [Fig. 4(a)]. The presence of harmonics became evident for $W = 3.45$ m and $L = 3.00$ m [Fig. 4(d)], and the corresponding dimensionless variables formed relatively parallel trends [Fig. 4(b)]. The curve that was derived from least-squares fitting in the data with no harmonics fitted very well the harmonics data from this example that had frequency approximately equal to 22.5 Hz, which is not the fundamental

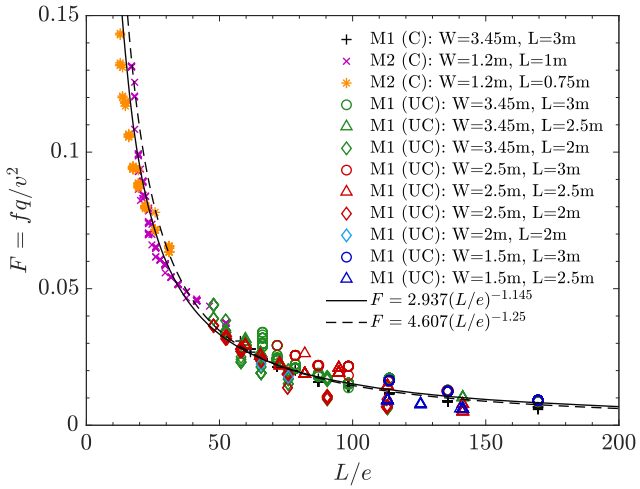

Fig. 2. Relationship between the ratio of the fall height to the water depth at the crest L/e and the dimensionless frequency of nappe oscillations F for weirs with a quarter round (QR) crest profile. In the legend, M1 and M2 denote Model 1 and Model 2, respectively, while C and UC in parentheses show if the nappe is confined or unconfined, respectively.

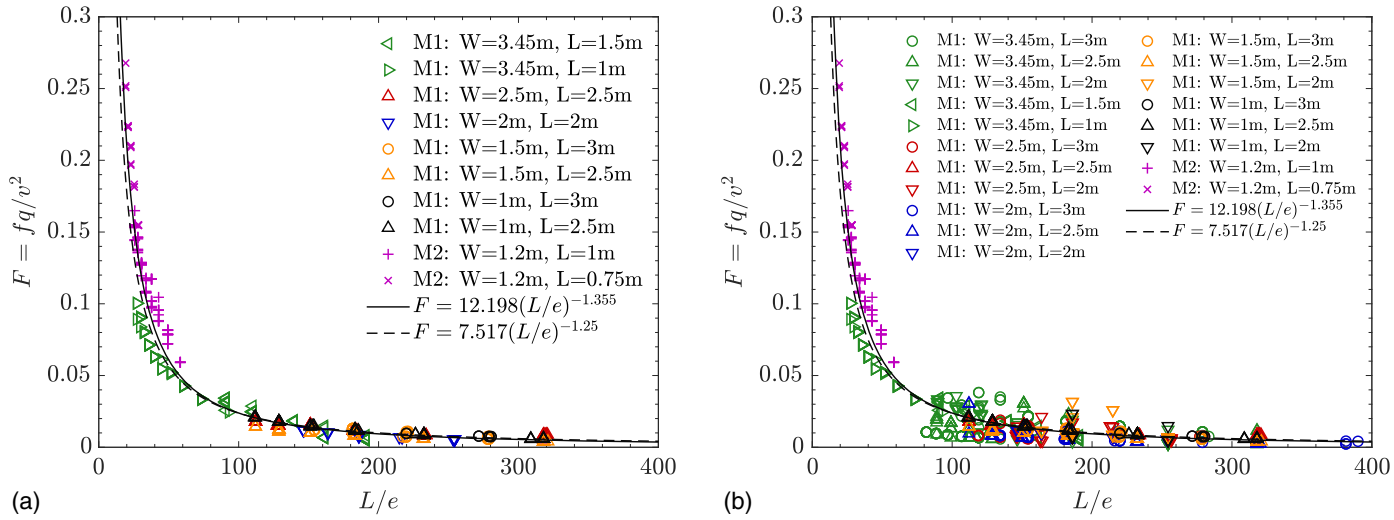

Fig. 3. Relationship between the ratio of the fall height to the water depth at the crest L/e and the dimensionless frequency of nappe oscillations F for weirs with a truncated half-round (THR) crest profile for (a) data with the THR crest without the presence of harmonics; and (b) all data with the THR crest. The curve depicted in both subfigures was fitted in the data of (a). In the legend, M1 and M2 denote Model 1 and Model 2, respectively. All configurations are with the nappe being confined.

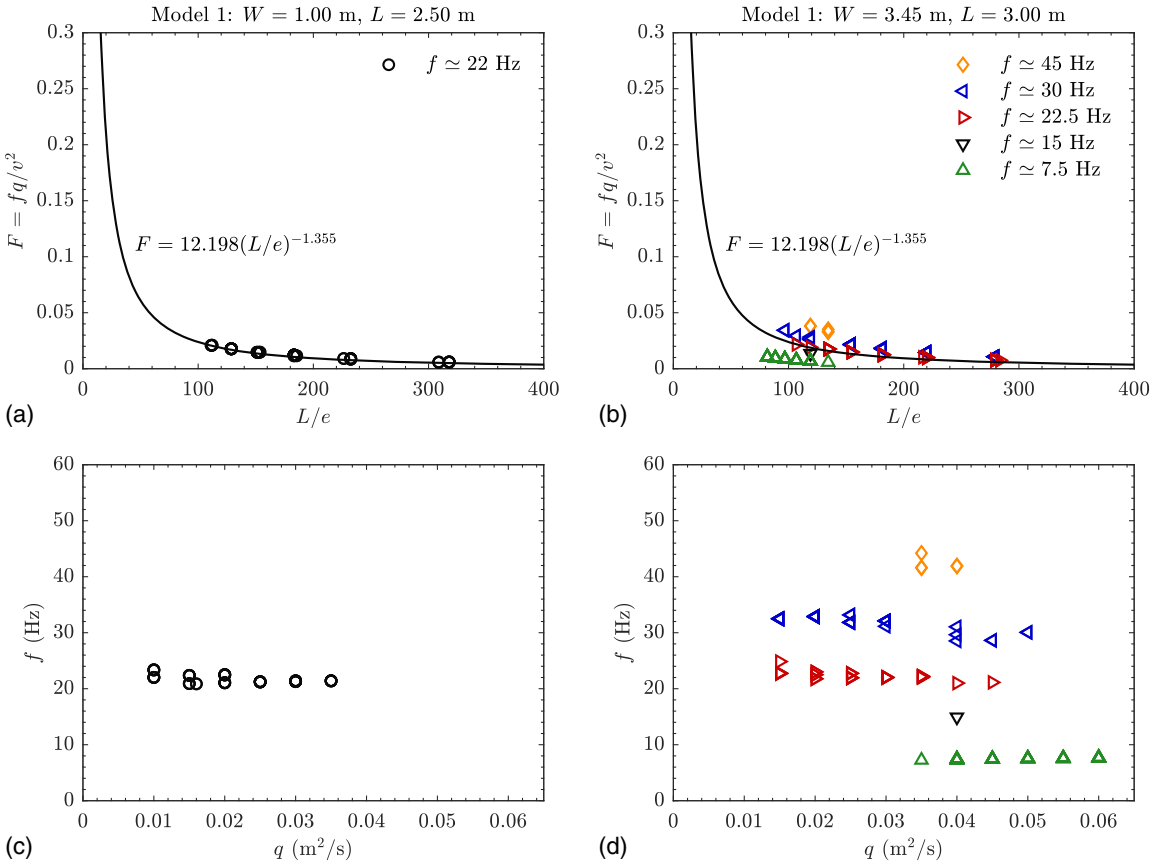

Fig. 4. Examples of relationships between L/e and F for weir geometries with a truncated half-round (THR) crest profile with (a) data from geometry that did not contain harmonics in their signals; (b) data from geometry that contained harmonics in their signals; and (c and d) similar data for the relationship between q and f.

frequency. The reason for this frequency preference is unclear and should be further explored in future research.

Notably, the exponents of the best-fit curves for the QR and THR crests are very close to each other, i.e., −1.145 and−1.355, respectively. The derived relationships could be further simplified by considering the average value of these two exponents, which is equal to −1.25, as a constant exponent, regardless if the crest type is QR or THR. The resulting R^2 is 0.88 for QR and 0.91 for THR,

and thus, the effect of the crest type on the relationship between F and L/e is solely to offset the curves for QR and THR.

Conclusion

Nappe oscillations occur in free surface weirs for relatively low hydraulic heads and can have an adverse impact to the surrounding environment and the structure itself. This study analyzed experimental data from two different experimental facilities with model weirs of different scales under various hydraulic and geometric conditions.

Nappe oscillations were observed at both scales for similar unit discharges between 0.01 and 0.06 m^2/s, confirming the fact that nappe oscillations cannot be modeled with Froude similarity. The weir crest geometry controls, to a large extent, whether nappe oscillations occur. Crests with geometric discontinuities at their upstream profile disturbed the flow substantially and inhibited the formation of nappe oscillations. On the contrary, an abrupt nappe detachment due to downstream discontinuities favored the formation of nappe oscillations, presumably due to sudden pressure change at the point of flow detachment. The confinement of the nappe was not necessary for nappe oscillations to occur.

A dimensionless nappe oscillations frequency, F, was expressed as a power function of the ratio of the fall height to water depth at the crest detachment point, L/e, for quarter-round and truncated half-round weir crests. The power function exponents for these two weir crests are close to each other, allowing the usage of their average value and the simplification of the power functions by considering a constant exponent as $F = a(L/e)^{-1.25}$, with a being an offsetting parameter depending on the crest type.

Data Availability Statement

All data generated or used during the study are available in a repository online (Lodomez et al. 2020).

Acknowledgments

Maurine Lodomez is grateful to the Fédération Wallonie-Bruxelles for funding her research visit to Utah State University and to Utah Water Research Laboratory for hosting her and enabling the tests on Model 2.

References

Anderson, A., and B. P. Tullis. 2018. "Finite crest length weir nappe oscillation." *J. Hydraul. Eng.* 144 (6): 04018020. https://doi.org/10.1061/(ASCE)HY.1943-7900.0001461.

Casperson, L. W. 1993. "Fluttering fountains." *J. Sound Vib.* 162 (2): 251–262. https://doi.org/10.1006/jsvi.1993.1117.

Chanson, H. 1996. *Some hydraulic aspects during overflow above inflatable flexible membrane dam.* Technical Rep. CH47/96. Brisbane, Australia: Univ. of Queensland.

Crookston, B. M., A. Anderson, L. Shearin-Feimster, and B. P. Tullis. 2014. "Mitigation investigation of flow-induced vibrations at a rehabilitated spillway." In *Proc., 5th Int. Symp. on Hydraulic Structures: Hydraulic Structures and Society—Engineering Challenges and Extremes*, 149–156. Brisbane, Australia: Univ. of Queensland. https://doi.org/10.14264/uql.2014.30.

De Rosa, F., M. Girfoglio, and L. de Luca. 2014. "Global dynamics analysis of nappe oscillation." *Phys. Fluids* 26 (12): 122109. https://doi.org/10.1063/1.4904752.

Girfoglio, M., F. De Rosa, G. Coppola, and L. de Luca. 2017. "Unsteady critical liquid sheet flows." *J. Fluid Mech.* 821: 219–247. https://doi.org/10.1017/jfm.2017.241.

Khodier, M. A., and B. P. Tullis. 2018. "PIV measurements for oscillating liquid nappe." *J. Hydro-environ. Res.* 19 (Mar): 237–242. https://doi.org/10.1016/j.jher.2017.11.002.

Lodomez, M., B. M. Crookston, B. P. Tullis, and S. Erpicum. 2019a. "Mitigation techniques for nappe oscillations on free-overfall structures." *J. Hydraul. Eng.* 145 (2): 04018086. https://doi.org/10.1061/(ASCE)HY.1943-7900.0001558.

Lodomez, M., M. Pirotton, B. Dewals, P. Archambeau, and S. Erpicum. 2018. "Nappe oscillations on free-overfall structures: Experimental analysis." *J. Hydraul. Eng.* 144 (3): 04018001. https://doi.org/10.1061/(ASCE)HY.1943-7900.0001420.

Lodomez, M., B. Tullis, P. Archambeau, V. Kitsikoudis, M. Pirotton, B. Dewals, and S. Erpicum. 2020. "Nappe oscillations on free-overfall structures: Data from laboratory experiments." *Sci. Data* 7 (1): 180. https://doi.org/10.1038/s41597-020-0521-8.

Lodomez, M., B. P. Tullis, B. Dewals, P. Archambeau, M. Pirotton, and S. Erpicum. 2019b. "Nappe oscillations on free-overfall structures: Size scale effects." *J. Hydraul. Eng.* 145 (6): 04019022. https://doi.org/10.1061/(ASCE)HY.1943-7900.0001615.

Naudascher, E., and D. Rockwell. 1994. *Flow-induced vibrations: An engineering guide*. Rotterdam, Netherlands: A.A. Balkema.

Petrikat, K. 1958. "Vibration tests on weirs and bottom gates." *Water Power* 10: 52–57.

Schmid, P. J., and D. S. Henningson. 2002. "On the stability of a falling liquid curtain." *J. Fluid Mech.* 463 (Jul): 163–171. https://doi.org/10.1017/S002211200200873X.

Schwartz, H. I. 1964. "Nappe oscillation." *J. Hydraul. Div.* 90 (6): 129–143.